Analytica Chimica Acta 1239 (2023) 340729

Contents lists available at ScienceDirect

Analytica Chimica Acta

journal homepage: www.elsevier.com/locate/aca

Fluorescent paper-based sensor integrated with headspace thin-film microextraction for the detection of acyclic N-nitrosamines following *in situ* photocatalytic decomposition

Vanesa Romero **, Carolina Sant'Anna, Isela Lavilla, Carlos Bendicho *

Centro de Investigación Mariña, Universidade de Vigo, Departamento de Química Analítica y Alimentaria, Grupo QA2, 36310, Vigo, Spain

HIGHLIGHTS

- *In situ* photocatalytic decomposition of *N*-nitrosamines to NO_x species is performed.
- Combination of microextraction with fluorescent paper-based sensing for NO_x detection.
- Ag NCs immobilized onto cellulose behave both as sorption and sensing platforms.
- Front-face fluorescence spectroscopy as readout technique in the paper-based sensor.
- A simple and rapid method for acyclic *N*-nitrosamines detection is accomplished.

GRAPHICAL ABSTRACT

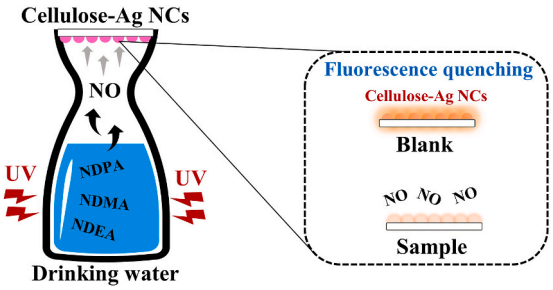

ARTICLE INFO

Keywords:
N-nitrosamines
Photocatalysis decomposition
Thin-film microextraction
Ag NCs fluorescent probes
Cellulose substrates
Drinking waters

ABSTRACT

Background: In this work, a novel analytical approach based on the photocatalytic decomposition of *N*-nitrosamines combined with headspace thin-film microextraction of the generated nitrogen oxides such as NO has been developed for the determination of the acyclic *N*-nitrosamine fraction in drinking water samples. A hydrophilic cellulose substrate modified with fluorescent silver nanoclusters (Ag NCs) was used both as extractant and sensing platform. A quenching effect of Ag NCs fluorescence occurs as the concentration of *N*-nitrosamines increases. Front-face fluorescence spectroscopy with a solid sample holder was employed for directly measuring the fluorescence quenching onto the cellulose substrate.

Results: In order to achieve an optimal analytical response, different parameters involved in the photocatalytic reaction as well as those concerning the microextraction step were fully investigated. It is demonstrated that the photodegradation rate of cyclic *N*-nitrosamines at acidic pH is much lower than that of acyclic ones, which can be the basis for the determination of the later fraction in waters. Under optimal conditions, a detection limit for the acyclic *N*-nitrosamine fraction around 0.08 μg L^{-1} using *N*-nitrosodimethylamine (NDMA) as model compound for calibration was obtained. Several drinking waters were spiked with acyclic *N*-nitrosamines showing recoveries in the range of 98–102% with a relative standard deviation of 3–4% (N = 3).

Significance and novelty: N-nitrosamines generated as by-products during disinfection processes applied to water cause multiple adverse effects on human health being classified as potential human carcinogens.

* Corresponding author.
** Corresponding author.
E-mail addresses: vromero@uvigo.es (V. Romero), bendicho@uvigo.es (C. Bendicho).

https://doi.org/10.1016/j.aca.2022.340729
Received 21 November 2022; Received in revised form 16 December 2022; Accepted 17 December 2022
Available online 20 December 2022

This study highlights the suitability of a fluorescent paper-based sensor for the rapid analysis of the acyclic *N*-nitrosamine fraction (*i.e.* the most abundant fraction) as a total index in drinking water, being useful as screening tool before exhaustive chromatographic analysis, which saves costs, time and reduces waste generation.

1. Introduction

Drinking water disinfection is of paramount importance to avoid waterborne diseases caused by pathogen microorganisms [1]. However, during the disinfection process, non-desirable by-products can be generated. This is the case of *N*-nitrosamines, *i.e.* nitrogen containing by-products, which are classified as potential human carcinogens. *N*-nitrosamines cause multiple adverse effects on human health, including hepatotoxicity, neurotoxicity, immunotoxicity, and genotoxicity [2]. These compounds can be also detected as pollutants in the aquatic environment due to anthropogenic discharges of untreated urban wastewater containing precursors, which originate *N*-nitrosamines by nitrosation [3]. Furthermore, it has been recently reported that *N*-nitrosamines and their precursors can be also release from tire scraps in high traffic areas [4], which can be dragged on rainy days reaching water sources. The composition and levels of *N*-nitrosamines in water relies on the characteristics of the water source and disinfection treatments. Usually, the concentration of *N*-nitrosamines in drinking water is in the range of ng L^{-1} [5,6]. Different *N*-nitrosamines have been detected in chloraminated drinking water and surface water, including *N*-nitrosodimethylamine (NDMA), *N*-nitrosodibutylamine (NDBA), *N*-nitrosodiethylamine (NDEA), *N*-nitrosomethylethylamine (NEMA), *N*-nitrosodipropylamine (NDPA), *N*-nitrosodiphenylamine (NDPhA), *N*-nitrosomorpholine (NMOR), *N*-nitrosopiperidine (NPIP), and *N*-nitrosopyrrolidine (NPYR). Among them, NDMA and NDEA are the most reported species, representing up to 60% of the total *N*-nitrosamines that can be found in drinking water and recycled water [5,7]. NDMA is included in the World Health Organization (WHO) Drinking Water Guidelines with a guideline value of 100 ng L^{-1} in drinking water. In the European Union, *N*-nitrosamines are not still specifically listed in the Drinking Water Directive (Council Directive 98/93/EC, revised in December 2020). Different countries have monitored the presence of *N*-nitrosamines in drinking and recycled water establishing notification levels for the most frequently found *N*-nitrosamines. For instance, the German regulatory authorities set a notification value of 10 ng L^{-1} for NDMA.

Direct detection of *N*-nitrosamines in water is difficult owing to their low concentrations. Hence, sample pre-treatment for enriching the target *N*-nitrosamines from water matrices and interference removal are usually employed. Solid phase extraction (SPE) [8–10] and its miniaturized versions, such as micro-solid phase extraction (μSPE), dispersive solid phase extraction (dSPE) [11], solid phase membrane tip extraction (SPMTE) [12], stir bar sorptive extraction (SBSE) [13] and thin film microextraction (TFME) [14] have been applied for sample clean-up and analyte pre-concentration due to their advantages of easy operation, ability to achieve high enrichment factors, efficient interference removal and low consumption of solvents. In combination with the above-mentioned sample treatment strategies, high performance liquid chromatography (HPLC) and gas chromatography (GC) coupled to mass spectrometry (MS) are the most used techniques for the detection of *N*-nitrosamines in water samples [15,16]. In fact, the normalized EPA Method 521 for the determination of *N*-nitrosamines in drinking water is based on the use of SPE followed by gas chromatography coupled to tandem mass spectrometry (GC-MS/MS) [17]. Despite these techniques offer high sensitivity, a desorption step is required in all cases prior to analysis apart from involving the use of expensive equipment requiring high level of expertise.

The integration of analyte separation/derivatization, enrichment and sensing in one only device would provide a very efficient and simplified analytical approach. In this sense, nanomaterials can be used as optical probes for recognition and enrichment of the target analyte simultaneously. Among the different nanomaterials, silver nanoclusters (Ag NCs) can be easily synthesized offering high photostability, good miscibility in aqueous media, good biocompatibility and efficient emission rate [18]. Ag NCs have been used as fluorescent sensors for the detection of a wide variety of analytes including metal ions [19,20], amino acids, *e.g.*, glutathione [21], volatile organic compounds, *e.g.*, formaldehyde [22], pharmaceuticals [23,24], and biomarkers such as uric acid, sarcosine, choline, lactic acid and glucose [25].

However, there are very few reports in the literature on the development of sensors for *N*-nitrosamines. For instance, Hu et al. developed a procedure based on the use of quantum dots (QDs) as fluorescence nanoprobe for the detection of NDPhA in tap water and seawater samples [26]. To reach good selectivity and ensure QDs stability in the sample matrix, molecularly imprinted polymers (MIPs) must be used as coating of QDs.

In order to avoid matrix interference or nanoprobe instability, it would be interesting to generate volatile species from *N*-nitrosamines, which can be detected or extracted in the gas phase, hence avoiding direct contact with the sample matrix. In this sense, it is known that the homolytic cleavage of the N–NO bond in *N*-nitrosamines by UV light yields nitrite (NO_2^-) [27], which can further converted into volatile nitrogen oxides, such as NO and N_2O [28]. Based on these reactions, molecular techniques such as UV–Vis spectrophotometry [29], fluorescence or chemiluminescence [30–32] in combination with chromatography have been employed for the determination of *N*-nitrosamines after derivatization of the photolysis products.

If UV irradiation is performed in a closed system, the generated NO can be extracted and preconcentrated following headspace (micro) extraction onto a sensing platform making it feasible the determination of total *N*-nitrosamines without the need for a desorption step or chromatographic separation. As far as we know, nanomaterials applied as optical nanoprobes for *N*-nitrosamines through the detection of NO after photolysis or photocatalysis, have not been reported yet. In this work, an innovative analytical approach based on the fluorescence detection of *N*-nitrosamines following photocatalysis in aqueous phase and headspace microextraction of NO onto a cellulose substrate modified with silver nanoclusters (Ag NCs) is developed. Application of the proposed method to the determination of the acyclic N-nitrosamines fraction including compounds such as NDMA NDEA, and NDPA in water samples is demonstrated.

2. Experimental

2.1. Instrumentation and material

Front-face fluorescence measurements were performed by means of a spectrofluorometer Horiba model Fluoromax-4 series (Tokyo, Japan) equipped with solid sample holder model J1933 maintaining an incidence angle of excitation at 60°. A microbalance model MC5 and an analytical balance model CP 124S (Sartorious, Göttingen, Germany) were used for weighing. A Metrohm UV digester model 705 (220 V, 50 Hz) equipped with high pressure mercury lamp (500 W) and sample tube holder with 12 positions (Herisau, Switzerland), was used for UV irradiation. Transmission electron microscopy (TEM) images were captured with a JEOL JEM-1010 instrument (Tokyo, Japan) for the characterization of Ag NCs and palladium nanoparticles.

Quartz tubes of 12.5 cm length and 15.6 mm external diameter (Metrohm AG, Herisau, Switzerland) were used as containers to perform photocatalysis and microextraction. Rubber septa 14.9 mm diameter

(Saint-Gobain, Charny, France) were used for closing the quartz tubes. Whatman™ quantitative filter paper grade 1 (pore size 11 μm, thickness 180 μm), grade 3 (pore size 6 μm, thickness 390 μm), grade 540 (pore size 8 μm, thickness 160 μm), grade 541 (pore size 22 μm, thickness 155 μm) and grade 542 (pore size 2.7 μm, thickness 150 μm) (GE Healthcare, Buckinghamshire, UK), were used as platforms for immobilization of Ag NCs.

2.2. Standards and reagents

All chemicals were of analytical reagent grade. Ultrapure water obtained from Merck Millipore Simplicity water system (Darmstadt, Germany) was used. For the synthesis of Ag NCs, silver nitrate 99% (m/m) (Scharlau, Barcelona, Spain) and poly(methacrylic acid sodium salt) (PMAA-Na) 40% m/v, average Mw 4000–6000 (Sigma-Aldrich, St Louis, USA) were used. Palladium nitrate dihydrate 40% Pd basis (Sigma-Aldrich, St Louis, USA) and absolute ethanol (Prolabo, Fontenay-sous-bois, France) were employed for the synthesis of palladium nanoparticles (Pd NPs). Formic acid 90.5% (m/m) (Merck, Darmstadt, Germany) and titanium dioxide nanopowder 99.7% (m/m) with and average particle size of 5 nm (Sigma-Aldrich, St Louis, USA) were used for photocatalysis. Stock standard solutions (500 mg L^{-1}) of NDEA (ISOPAC®, Sigma-Aldrich, Tokyo, Japan) and NPYR (Fluorochem, Castleton, UK) were prepared by diluting the commercial *N*-nitrosamines in methanol. NDMA, NDPA, NMOR and NPIP 500 mg L^{-1} certified reference material solutions in methanol (CRM40059, CRM40061, CRM40458 and CRM40485, respectively) were purchased from Sigma-Aldrich (St. Louis, USA). Diluted working aqueous standards were prepared fresh daily from the stock solutions.

The following reagents were employed for interference studies: sodium chloride 99.5% (m/m) (Sigma-Aldrich, Soborg, Denmark), sodium sulphate 99% (m/m) (Sigma-Aldrich, Bangalore, India), magnesium chloride hexahydrate 99% (m/m), potassium dihydrogen phosphate 99% (m/m), calcium sulphate dihydrate 99% (m/m) (Merck, Darmstadt, Germany), sodium hydrogen carbonate 99.8% (m/m) (Carlo Erba, Rodano, Italy), sodium carbonate anhydrous 99.5% (m/m) (Panreac, Barcelona, Spain) and humic acid (Fluka, Buchs, Switzerland).

2.3. Experimental procedure

2.3.1. Synthesis of Ag NCs and W1–Ag substrates preparation

Ag NCs were synthesized following the procedure described by Lu et al. [33] with few modifications. Briefly, 60 mg of $AgNO_3$ (0.35 mmol) were dissolved in 4 mL in ultrapure water at pH 7.2. The aqueous solution was transferred to a quartz tube (15.6 mm Ø, 12 mL capacity) and 0.2 mL of PMAA-Na were added. The mixture was homogenized by vortex mixing for 30 s. Finally, the quartz tube was placed in the UV digester and irradiated for 15 s. The solution changed from colourless to dark pink. The synthesized Ag NCs were kept in an amber glass vial at 4 °C before use. This colloidal solution was stable for at least five months.

To prepare the cellulose substrates containing Ag NCs, firstly Whatman™ quantitative filter paper grade 1 (pore size 11 μm, thickness 180 μm) were cut in 8 mm diameter circles using a hole punch. This diameter fits well with the size of the septum used for closing the quartz tubes. Ag NCs were deposited onto the cellulose substrate by the drop-casting method. For this, an aliquot of 10 μL Ag NCs was added onto the cellulose substrate (W1) and dried in the dark in a laminar flow hood at room temperature for 1 h. The obtained dried substrates, named as W1–Ag, were stored at room temperature in plastic petri dishes covered with aluminum foil for protecting from light until use. These substrates were stable for at least 5 days.

2.3.2. Synthesis of Pd NPs

Uncoated Pd NPs, used as metal catalyst for the photodecomposition of *N*-nitrosamines, were synthesized following the procedure describe by Romero et al. [34]. Briefly, 1.5 mg of $Pd(NO_3)_2{\cdot}2H_2O$ were dissolved in 300 μL of a water:ethanol mixture (1:2 v/v). The mixture was undisturbed for 10 min until the solution changes from light yellow to black color indicating the formation of colloidal Pd with an average particle size of 3 nm. These Pd NPs were prepared daily.

2.3.3. Photocatalytic decomposition of nitrosamines and headspace thin-film microextraction

For the photocatalysis of *N*-nitrosamines and fluorescence sensing, 8 mL of aqueous solution (sample, standard or blank) containing 1 M formic acid, 0.2 mg mL^{-1} TiO_2 and 0.3 μg mL^{-1} Pd NPs, were added to a quartz tube containing a magnetic stirrer. The tube was closed with a rubber septum, which contains the W1–Ag substrate in the inner part of the septum (Fig. 1). Then, the tube was irradiated by UV light for 90 s so as to perform the photocatalytic decomposition of nitrosamines and the generation of volatile NO. Based on studies regarding photolysis of nitrosamines and photoreduction of nitrite [27,28,35,36], the following mechanism can be proposed to explain the formation of NO from *N*-nitrosamines:

$$R-N-N=O\cdots H^{+}\xrightarrow{h\nu}(R-N-N=O)^{*}_{excited\ state}\xrightarrow{H_2O/H^{+}}R-NH_2^{+}+HNO_2 \quad (1)$$

$$HNO_2 \leftrightarrow NO_2^{-}+H^{+} \quad (2)$$

$$NO_2^{-}+e^{-}_{TiO_2}\xrightarrow[h\nu]{HCOOH-Pd}NO_2^{\bullet\,2-} \quad (3)$$

$$NO_2^{\bullet\,2-}+2H^{+}\rightarrow\ \uparrow \mathrm{NO}+H_2O \quad (4)$$

N-nitrosamines are known to undergo photolysis under acidic conditions. The photoexcited protonated *N*-nitrosamine can be converted to nitrous acid under UV light (1), which further decomposes to nitrite (2). In addition, TiO_2 generates simultaneously electrons ($e^{-}_{TiO_2}$) and holes (h^{+}) when irradiated by UV light [37]. Under acidic conditions, nitrite is reduced to $NO_2^{\bullet\,2-}$ radical (3) followed by a subsequent dehydration to volatile NO (4). In this step, formic acid (HCOOH) acts as hole scavenger enhancing the photoreduction of nitrite. Furthermore, the presence of a noble metal, such as Pd, can promote the rapid transfer of the photogenerated $e^{-}_{TiO_2}$ thus increasing the photocatalytic efficiency.

After UV irradiation, the tube was magnetically stirred for 2 min at 1600 rpm for a quick transfer of the NO to the W1–Ag substrate, which is exposed to the headspace. Finally, the W1–Ag substrate is collected and the fluorescence signal is measured using an excitation wavelength of 520 nm and an emission wavelength of 610 nm.

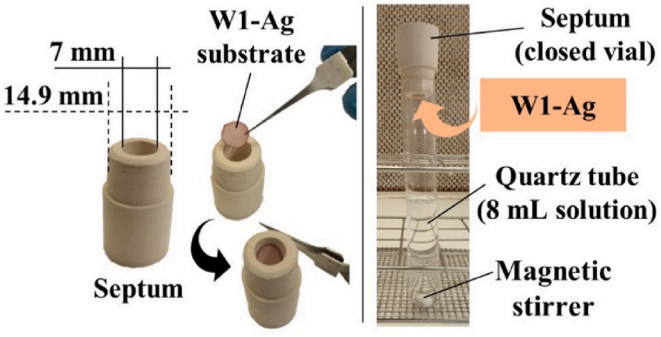

Fig. 1. W1–Ag substrate for HS-TFME of NO.

3. Results and discussion

3.1. Characterization and stability of Ag NCs

Firstly, optimal excitation and emission wavelengths for fluorescent measurements with Ag NCs were established. As can be seen in the 3D fluorescence spectrum for the Ag NCs (Fig. S1a, supplementary material), the highest fluorescence intensity is achieved for an excitation wavelength of 520 nm and an emission wavelength of 610 nm. These values were further selected for fluorescence measurements with the W1–Ag substrates. Furthermore, the Ag NCs were characterized by transmission electron microscopy (TEM) showing spherical shape with an average size of 3 nm (Fig. S1b).

Besides, the stability of the Ag NCs stored in amber glass vials at 4 °C was tested by measuring the fluorescence intensity for several months. As shown in Fig. S1c, there is no any significant change in the fluorescence signal at least for a period of 5 months, hence demonstrating the high stability of the as-prepared Ag NCs. In addition, Whatman-1 cellulose substrates before and after Ag NCs drop-casting are shown in Fig. S1d. As can be seen, W1–Ag substrates show orange fluorescence under UV irradiation, which is indicative of the formation of Ag-PMAA NCs [33].

3.2. Preliminary studies

Before optimization of the parameters involved in both photocatalysis and microextraction steps, several preliminary studies were carried out. It has been reported that *N*-nitrosamines photolysis yield nitrite as intermediate species, which is further photoreduced giving rise to NO [27,38]. Taking this into account, nitrite at a 0.5 μg mL^{-1} concentration was used for preliminary studies and optimizations since its toxicity and cost is lower as compared to *N*-nitrosamines. The analytical response is expressed as the fluorescence intensities ratio of the blank (I_0) and standard signal (I).

In order to establish the reaction conditions, a photolysis step (without a catalyst) was firstly attempted. For this, two different short chain carboxylic acids, *e.g.*, formic acid and acetic acid, used as H_2 precursors in photoreduction reactions [39], have been tested. Fluorescence was recorded both for blanks and standards immediately after UV irradiation. As shown in Fig. 2a, both acids increase the reaction kinetics resulting in higher fluorescence quenching in comparison with the results obtained without a precursor. It should be noted that when acetic acid is used, some condensation is observed in the upper part of the quartz tube (headspace) resulting in poor precision. Therefore, formic acid was selected as H_2 precursor for further optimization studies.

In addition, stirring during the microextraction step favors the mass transfer as well as convection in the headspace, thus facilitating the extraction of the volatile species generated (Fig. S2). As shown, magnetic stirring during the microextraction step results in a significant increase in the analytical response (quenching) when compared to the results obtained without stirring. On the other hand, during mechanical agitation (*e.g.* using a vortex), the liquid phase can reach the W1–Ag substrate exposed to the headspace, causing impaired results. Thus, magnetic stirring at 1600 rpm was used for further studies.

For assessing the influence of the cellulose substrate used for preparing the extractant phase, several Whatman™ filter papers, *i.e.* grade 1, grade 3, grade 540, grade 541 and grade 542, with different pore size and thickness were tested. Substrates were prepared following the procedure described in section 2.3.1. As can be seen in Fig. 2b, those filter papers with higher thickness, *i.e.*, Whatman™-3 and Whatman™-542, showed worse analytical response, which can be ascribed to lower extraction kinetics. In this case, it was necessary to increase the extraction time for achieving higher analytical response [40]. On the other hand, for filter papers with similar thickness, *i.e.*, Whatman™-540, Whatman™-1 and Whatman™-541, the results improve as the pore size increases. A larger pore size can facilitate the analyte diffusion in the extracting phase, thus increasing the analyte response obtained [41]. Consequently, the filter paper Whatman™-1 was selected for further studies.

The amount of Ag NCs on the cellulose substrate, which determines the fluorescence signal and subsequently the analytical response, directly depends on the volume of the deposited aliquot. The aliquot should impregnate completely the cellulose substrate ensuring the homogeneous distribution of the Ag NCs. In order to evaluate the influence of this parameter on the analytical response, different volumes in the range from 2 μL to 20 μL were deposited on the Whatman™-1 substrates (Ø 10 mm). Results are shown in Fig. 2c. The analytical response increases on increasing volume of Ag NCs deposited up to 10 μL. For small volumes of Ag NCs, the cellulose substrate is not completely coated with Ag NCs resulting in poor fluorescence intensity and thus low analytical response. For volumes above 10 μL, lower analytical responses are obtained, which can be ascribed to the O-ring effect, *i.e.*, Ag NCs are not homogeneously distributed being mostly accumulated at the cellulose substrate boundaries, worsening the fluorescence intensity and thus the precision. Furthermore, 20 μL aliquot exceed the cellulose substrate boundaries resulting in Ag NCs losses. Finally, a 10 μL aliquot was chosen as optimal.

3.3. Optimization of experimental parameters

Different parameters involved in the photocatalysis procedure (NO generation) and the microextraction step were optimized. Experiments were carried out using 0.1 μg mL^{-1} nitrite. The analytical response is expressed as the ratio between the fluorescence intensity of the blank (I_0) and the standard signal (I).

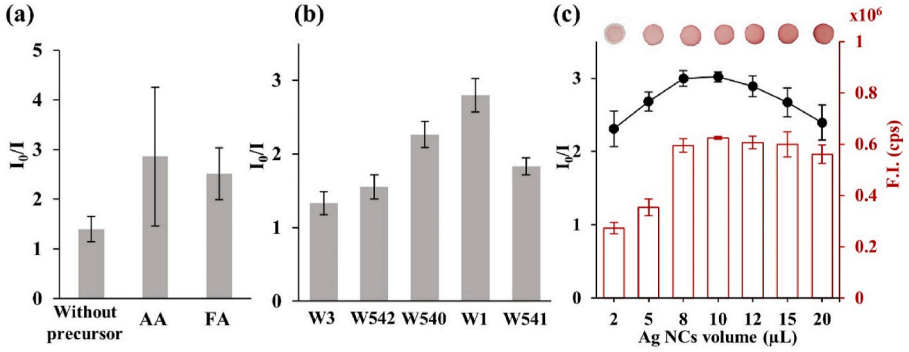

Fig. 2. (a) Type of H_2 precursor (AA: acetic acid; FA: formic acid); **(b)** Type of Whatman™ cellulose substrate type (W3: Whatman™ grade 3; W542: Whatman™ grade 542; W540: Whatman™ grade 540; W1: Whatman™ grade 1; W541: Whatman™ grade 541); **(c)** Volume of Ag NCs deposited on the cellulose substrate (volume range: 2–20 μL corresponding to Ag NCs mass between 17 ng and 172 ng) (F.I.: fluorescence intensity).

3.3.1. Effect of the photocatalyst type and concentration

The use of photocatalysts in the reaction medium can favor the decomposition of formic acid as well as the generation of NO [42]. TiO_2 is one of the most used photocatalysts for the photoreduction of nitrites and nitrates [43]. Since nitrite is an intermediate species in the photolysis of *N*-nitrosamines, TiO_2 is expected to be a suitable photocatalyst for the proposed procedure. Furthermore, it has been reported that the combination with noble metals, such as Pd and Pt, increases the catalytic activity of TiO_2 [44]. In this work, nanostructured Pd (Pd nanoparticles, Pd NPs) was selected as metal catalyst, since it can provide increased surface area yielding higher reactivity [45].

Firstly, to evaluate their catalytic behavior, 0.5 mg mL^{-1} TiO_2 and 0.7 μg mL^{-1} Pd NPs were tested both separately and combined. As shown in Fig. 3a, the best analytical response is obtained when both photocatalysts are used simultaneously, thus demonstrating the synergistic effect. Then, to set the optimal amount of each photocatalyst in the reaction medium, concentrations in range of 0.05–1 mg mL^{-1} for TiO_2 and 0.05–1.5 μg mL^{-1} for Pd NPs, were studied. As can be observed in Fig. 3b, the analytical response increases on increasing the catalyst concentration up to 0.2 mg mL^{-1} TiO_2 and 0.3 μg mL^{-1} Pd NPs. These concentrations were selected for further studies.

3.3.2. Effect of UV irradiation time and formic acid concentration

UV irradiation is a critical parameter that affects the decomposition of formic acid releasing H_2 [46] as well the formation of free radicals, which induce the photocatalytic decomposition of nitrosamines to yield NO [27]. To evaluate the effect of this parameters, different UV irradiation times were tested (Fig. 3c). As the UV irradiation time increases, the response is higher, since the photoreaction kinetics is enhanced, until reaching a maximum at 90 s. For longer UV irradiation times, condensation in the upper part of the quartz tube was observed. The W1–Ag substrate can get wet, yielding lower fluorescence signal of Ag NCs for both blanks and standards. An UV irradiation time of 90 s was selected as optimal for further optimizations.

Besides, the concentration of formic acid was tested in the range of 0.1–1.2 M. The obtained results are shown in Fig. 3d. The analytical response increases with increasing formic acid concentration up to 0.8 M. For higher concentrations, the quenching signal keeps constant. Hence, a formic acid concentration of 1 M was selected.

3.3.3. Effect of sample volume

In order to evaluate the effect of sample volume, different volumes in the range of 1–10 mL were tried. An increase in the sample volume brings about a decrease in the headspace sample volume, and hence, the higher concentration of volatile species achieved would entail an enhanced sensitivity [47]. This positive effect is observed up to a sample volume of 8 mL (Fig. 4a). For larger sample volumes, a decrease in the analytical response occurs, which can be attributed to a lower convection of the aqueous phase during microextraction [48]. Therefore, a sample volume of 8 mL was selected as optimal.

3.3.4. Effect of microextraction time

The time needed to reach equilibrium conditions during the microextraction process is crucial for an efficient mass transfer of volatile species from the headspace to the W1–Ag substrate. Different microextraction times from 30 s to 6 min were tested. As can be seen in Fig. 4b, the analytical signal increases rapidly reaching a plateau at 2 min. In accordance with these results, a microextraction time of 2 min was chosen as optimal.

3.4. N-nitrosamines sensing

To evaluate the application of the proposed method, photocatalysis and HS-TFME of six different *N*-nitrosamines, *i.e.* 1-nitrosopyrolidine (NPYR), *N*-nitrosomorpholine (NMOR), *N*-nitrosopiperidine (NPIP), *N*-nitrosodimethylamine (NDMA), *N*-nitrosodiethylamine (NDEA), and *N*-nitrosodipropylamine (NDPA) were carried out under optimal conditions. NDMA, NDEA and NDPA were selected as the most representative of the acyclic *N*-nitrosamines family, whereas NPYR, NMOR and NPIP were selected as a model of cyclic *N*-nitrosamines. The analytical response of each *N*-nitrosamine is shown in Fig. 4c. NDEA, NDMA and NDPA provided comparable analytical response showing a similar photodegradation efficiency. On the other hand, cyclic *N*-nitrosamines, NPYR, NMOR and NPIP, provided a negligible quenching ($I_0/I \sim 1.0$) of

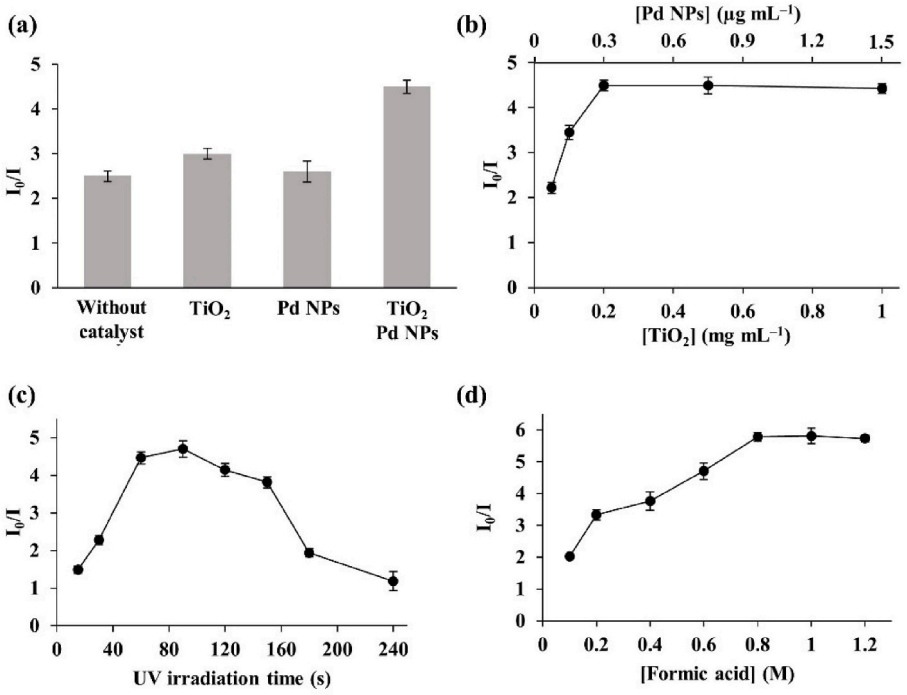

Fig. 3. **(a)** Effect of the type of photocatalyst; **(b)** Effect of TiO_2 and Pd NPs concentration as photocatalysts; **(c)** Effect of UV irradiation time; **(d)** Effect of formic acid concentration.

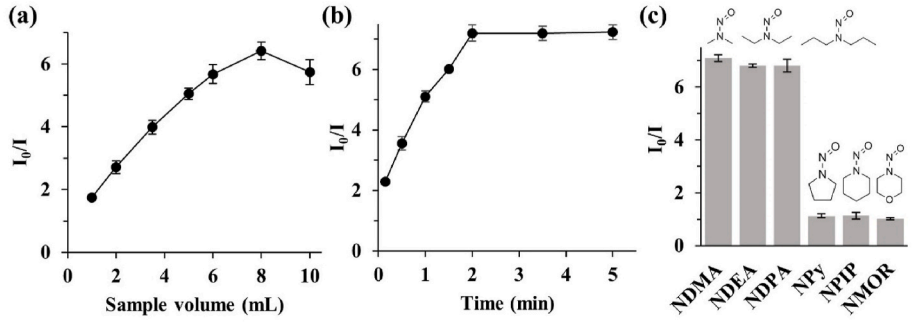

Fig. 4. **(a)** Effect of sample volume; **(b)** Effect of microextraction time; **(c)** *N*-nitrosamines response under optimal conditions (NDMA: *N*-nitrosodimethylamine; NDEA: *N*-nitrosodiethylamine; NDPA: *N*-nitrosodipropylamine; NPy: *N*-nitrosopyrrolidine; NPIP: *N*-nitrosopiperidine; NMOR: *N*-nitrosomorpholine).

the fluorescence signal. The photodegradation rate at acidic pH of cyclic *N*-nitrosamines is much lower than that of acyclic ones, due to their higher electron density and higher N–N band energy [49]. Therefore, the proposed method can be applied for the determination of the acyclic fraction of *N*-nitrosamines.

As mentioned before, *N*-nitrosamines are photosensitive and UV irradiation promotes the cleavage of the N–N bond yielding nitrite as intermediate species, which is further photoreduced to volatile nitrogen oxides, mainly NO [27,38]. It has been reported that NO can reacts with silver causing the reduction of volatile NO, most probably to N_2 [50,51]. In the proposed procedure, this interaction can promote the agglomeration of Ag NCs exposed to the headspace of the quartz vial with the subsequent loss in fluorescence intensity. Furthermore, oxygen-containing groups could enhance the redox activity towards NO. It is reported that NO interacts with the C═O bond of carboxylic acid groups [52]. In our case, the Ag NCs are coated with poly(methacrylic acid (PMAA), which possesses carboxylic groups, thus offering active sites available for interaction with NO.

3.5. Interference studies

Drinking water contain salts and organic matter that could interfere in the photocatalysis and/or microextraction processes. The potential interferent effect of different typical salts and organic matter (humic acid), which can be present in water samples, was tested (Table S1, supplementary material). An interferent effect was defined to be significant if a variation beyond ±6% in the quenching signal is observed. The experiments were performed at different concentration levels using: NaCl, Na_2SO_4, $MgCl_2$, $CaSO_4$, $NaHCO_3$, Na_2CO_3 (concentration in the range of 50–500 mg L^{-1}), KH_2PO_4 (concentration in the range of 5–50 mg L^{-1}), Na_2SO_3 (concentration in the range of 5–100 mg L^{-1}), $NaNO_3$ (concentration in the range of 1–50 mg mL^{-1}) and humic acid (concentration in the range of 1–20 mg L^{-1}). No interferences were observed. It should be noted that, under the conditions used in this work, inorganic species such as sulfite or nitrate, which could be decomposed to SO_x or NO_x volatile compounds under UV irradiation do not produce significant changes in the analytical signal, even at concentrations above the maximum permissible for drinking waters. Only high contents of NaCl (concentration above 250 mg L^{-1}) caused a significant decrease of around 8% in the analytical response. This depressive effect can be attributed to the formation of $Cl^{\bullet}$ radicals, which strongly absorbs UV photons, hence decreasing the fraction of UV absorbed by water [53]. Nonetheless, the NaCl concentration usually present in drinking water is lower than the tolerance level [54]. The Environmental Protection Agency (EPA) establishes a guidance level of 20 mg L^{-1} for Na in drinking water [55]. It can be concluded that this sensing approach exhibits great tolerance to matrix concomitants usually present in drinking waters.

3.6. Analytical figures of merit

The quenching effect produced by NO generated from the photocatalytic decomposition of *N*-nitrosamines is well described by the Stern-Volmer equation:

$$I_0/I = K_{sv}[Q] + C$$

where I_0 is the fluorescence intensity of the W1–Ag substrate after photocatalysis in the absence of *N*-nitrosamines (blank), I is the fluorescence intensity of the W1–Ag substrate after quenching, K_{sv} is the Stern-Volmer constant, Q is the concentration of *N*-nitrosamine in μg L^{-1}, and C is a constant. The analytical characteristics of the proposed method were established under optimal conditions. The calibration curves, based on the detection of NO generated from NDMA, NDEA and NDPA, were linear in the concentration range 2–120 μg L^{-1} for the three tested *N*-nitrosamines with correlation coefficients >0.99 (Fig. S3). Detection limits (LODs) calculated following the 3σ criterion, were around 0.08 μg L^{-1} for NDEA, NDMA and NDPA. The repeatability tested at a concentration of 50 μg L^{-1} expressed as relative standard deviation (RSD, N = 5) was 3.5% for the assessed analytes. The reproducibility estimated as between-day precision was 6.1% (N = 3). A comparison of the proposed methodology with other reported procedures for the determination of *N*-nitrosamines in water is shown in Table 1.

One of the main advantages of using immobilized Ag NCs onto cellulose substrates for sensing volatile *N*-nitrosamines after their photocatalytic decomposition is the absence of a desorption step before measurement, which saves time, solvents and reduces waste generation. Fluorescence intensity can be measured directly on the W1–Ag substrate using a solid sample holder (Fig. S4). Photocatalysis and microextraction can be accomplished in the same device within 3.5 min (1.5 min for photocatalysis +2 min for microextraction). Furthermore, using the UV digester for the photocatalysis step, up to 12 samples can be simultaneously treated, thus achieving a high sampling throughput. The use of HS-TFME for the preconcentration avoids the direct contact of the sensor with the sample matrix, which removes potential interferent effects. SPE approaches for purification and extraction of the target analytes are not needed. However, in contrast to chromatographic techniques, which allow to quantitate individual *N*-nitrosamines, only the total content of *N*-nitrosamines can be determined with the proposed methodology. Comparing the LODs for NDEA, NDMA and NDPA, the values obtained in the present work are significantly improved in comparison with those obtained by HPLC with post-column UV photolysis and UV photolysischemiluminescence.

4. Analysis of drinking water

Different drinking waters, *i.e.* mineral water, tap water and urban drinking fountain, were analyzed. Results for each acyclic *N*-nitrosamine tested separately are shown in Table 2. As can be seen, NDEA, NDMA or

Table 1
Comparison of different methods from the literature for the determination of NDMA, NDEA and NDPA in drinking water.

Analytical method	LOD (μg L^{-1})			Extraction time (min)	Desorption step	Repeatability (%)	Ref.
	NDMA	NDEA	NDPA				
μSPE-GC-EI-MS/MS	0.17	0.02	0.02	15	Liquid desorption	5	[8]
TFME-GC-MS	0.010	0.002	–	30	Thermal desorption	5	[14]
SPE-HPLC-PCUV	3.4	4.5	4.8	n.d.	Liquid desorption	10	[29]
UV photolysis-CL	5.2	8.2	9.1	3	Not required	6	[31]
SPE-HPLC-MS/MS	0.0004	0.002	0.0003	55	Liquid desorption	n.d.	[56]
SPE-HPLC-MS/MS	0.0002	0.0002	–	50	Liquid desorption	1.5	[57]
SPE-HPLC-UV photolysis-CL	0.0002	–	–	n.d.	Liquid desorption	n.d.	[58]
SBSE-GC-MS	–	2.8	2.4	25	Liquid desorption	6	[59]
UV photocatalysis-TFME-FL	0.08	0.09	0.08	3.5	Not required	3.5	This work

μSPE: micro-solid phase extraction; GC-EI-MS/MS: gas chromatography-electron ionization-mass spectrometry tandem; TFME: thin film microextraction; GC/MS: gas chromatography-mass spectrometry; SPE: solid phase extraction; HPLC-PCUV: high-performance liquid chromatography with post-column UV photolysis; CL: chemiluminescence; HPLC-MS/MS: high performance liquid chromatography-mass spectrometry tandem; SBSE: stir bar sorptive extraction; FL: fluorescence.

Table 2
Found values and recoveries obtained by applying the proposed approach for the analysis of different drinking water samples.

Sample	*N*-nitrosamine added (μg L^{-1})	*N*-nitrosamine found (μg L^{-1}) ± s (N = 3) (Recovery % ± s (N = 3)		
		NDMA	NDEA	NDPA
Drinking water-1	0	< LOD	<LOD	<LOD
	10	10.2 ± 0.4 (102 ± 3)	9.9 ± 0.4 (99 ± 4)	10.1 ± 0.3 (101 ± 3)
	25	25.2 ± 0.8 (101 ± 3)	25.1 ± 0.7 (100 ± 3)	24.9 ± 0.8 (100 ± 3)
	50	50.8 ± 1.5 (102 ± 5)	49.8 ± 1.9 (100 ± 4)	50.1 ± 1.7 (100 ± 3)
Drinking water-2	0	< LOD	<LOD	<LOD
	10	9.8 ± 0.3 (98 ± 3)	10.1 ± 0.3 (101 ± 3)	9.7 ± 0.4 (97 ± 4)
	25	24.9 ± 0.8 (100 ± 4)	24.8 ± 0.9 (99 ± 4)	25.2 ± 1.0 (101 ± 4)
	50	50.1 ± 1.2 (100 ± 4)	49.7 ± 2 (99 ± 4)	50.0 ± 1.8 (100 ± 4)
Tap water	0	< LOD	<LOD	<LOD
	10	10.1 ± 0.3 (101 ± 3)	10.0 ± 0.3 (100 ± 3)	9.9 ± 0.3 (99 ± 3)
	25	25.3 ± 0.7 (101 ± 3)	24.8 ± 1.1 (99 ± 4)	24.8 ± 0.8 (99 ± 3)
	50	50.5 ± 1.5 (101 ± 4)	49.1 ± 2.1 (98 ± 4)	49.6 ± 1.3 (99 ± 3)
Urban drinking fountain water	0	< LOD	<LOD	<LOD
	10	10.1 ± 0.4 (101 ± 4)	9.9 ± 0.4 (99 ± 4)	9.9 ± 0.3 (99 ± 3)
	25	24.8 ± 0.7 (99 ± 3)	24.5 ± 1.0 (98 ± 4)	25.2 ± 0.9 (101 ± 4)
	50	49.7 ± 1.6 (99 ± 3)	50.3 ± 2.0 (101 ± 4)	50.2 ± 1.7 (100 ± 3)

NDMA: *N*-nitrosodimethylamine; NDEA: *N*-nitrosodiethylamine; NDPA: *N*-nitrosodipropylamine.

NDPA were not detected in all cases. Furthermore, recovery studies were performed by spiking water samples at three concentration levels, *i.e.*, 10 μg L^{-1}, 25 μg L^{-1} and 50 μg L^{-1}, for selected acyclic *N*-nitrosamines. Average recoveries (%, N = 3) varied from 97% to 103% (Table 2).

In addition, recovery studies were carried out by spiking the Drinking Water-1 sample with a mixture of acyclic and cyclic *N*-nitrosamines, *i.e.* NDEA, NDMA, NDPA (as acyclic fraction) and NPYR, NMOR, NPIP (as cyclic fraction), at equal concentration of each individual compound. Total content of acyclic *N*-nitrosamines fraction was determined using NDMA as model compound for calibration since it is the most representative compound of the acyclic fraction, and the change in calibration curve slope is only 0.2% in respect to the mixture (Fig. S3). Results are shown in Table 3.

Table 3
Found values and recoveries obtained by applying the proposed approach in a water sample spiked with a mixture of *N*-nitrosamines. Recovered contents are expressed as NDMA concentration.

Sample	Acyclic *N*-nitrosamine mixture added (μg L^{-1})[a]	Acyclic *N*-nitrosamine found (μg L^{-1}) ± s (N = 3) (Recovery % ± s (N = 3)
		(as NDMA concentration)
Drinking water-1	15	15.1 ± 0.2 (101 ± 2)
	30	29.8 ± 0.5 (99 ± 2)
	60	59.7 ± 1.8 (99 ± 3)

[a] Total concentration as the sum of each individual acyclic *N*-nitrosamine at equal concentration. The cyclic fraction was added at equal concentration.

5. Conclusions

The proposed sensing approach based on the photocatalytic decomposition of *N*-nitrosamines and HS-TFME using cellulose substrates modified with Ag NCs (W1–Ag) both as extraction phase and fluorescence sensing platform has proven suitable for the determination of the acyclic N-nitrosamine fraction as a total index in water samples. *N*-nitrosamines can be directly quantitated on the W1–Ag substrate using front-face fluorescence spectroscopy. The integration of analyte derivatization, separation, enrichment and sensing in one only device provides an efficient and simplified approach. This approach could be useful for fast screening of the most abundant fraction of *N*-nitrosamines in drinking water prior to more sophisticated methods involving chromatographic separations along with mass spectrometry detection.

Funding

The authors thank the 'Ministerio Español de Ciencia e Innovación', the 'Agencia estatal de investigación' and FEDER (Project RTI2018-093697-B-I00) for financial support. Xunta de Galicia within the I2C postdoctoral program [grant number ED481D-2021-021]; Funding for open access charge: Universidade de Vigo/CISUG.

CRediT authorship contribution statement

Vanesa Romero: Conceptualization, Investigation, Writing – original draft. **Carolina Sant'Anna:** Investigation, Methodology. **Isela Lavilla:** Data curation, Writing – original draft. **Carlos Bendicho:** Conceptualization, Supervision, Writing – review & editing, Funding acquisition.

Declaration of competing interest

The authors declare that they have no known competing financial

interests or personal relationships that could have appeared to influence the work reported in this paper.

Data availability

Data will be made available on request.

Acknowledgements

The authors thank the CACTI facilities (University of Vigo) for assistance with the TEM measurements. This article is based upon work from the Sample Preparation Study Group and Network, supported by the Division of Analytical Chemistry of the European Chemical Society.

Appendix A. Supplementary data

Supplementary data to this article can be found online at https://doi.org/10.1016/j.aca.2022.340729.

References

[1] S. Tsitsifli, V. Kanakoudis, Disinfection impacts to drinking water safety-A review, Proceedings 2 (2018) 603, https://doi.org/10.3390/proceedings2110603.
[2] A.J. Gushgari, R.U. Halden, Critical review of major sources of human exposure to N-nitrosamines, Chemosphere 210 (2018) 1124–1136, https://doi.org/10.1016/j.chemosphere.2018.07.098.
[3] B. Zhao, Y. Wong, M. Ihara, N. Nakada, Z. Yu, Y. Sugie, J. Miao, H. Tanaka, Y. Guan, Characterization of nitrosamines and nitrosamine precursors as non-point source pollutants during heavy rainfall events in an urban water environment, J. Hazard Mater. 424 (2022), 127552, https://doi.org/10.1016/j.jhazmat.2021.127552.
[4] W. Beita-Sandí, M. Selbes, M.S. Ersan, T. Karanfil, Release of nitrosamines and nitrosamine precursors from scrap tires, Environ. Sci. Technol. Lett. 6 (2019) 251–256, https://doi.org/10.1021/acs.estlett.9b00172.
[5] M.J. Farré, S. Insa, A. Lamb, C. Cojocariu, W. Gernjak, Occurrence of: N-nitrosamines and their precursors in Spanish drinking water treatment plants and distribution systems, Environ. Sci. Water Res. Technol. 6 (2020) 210–220, https://doi.org/10.1039/c9ew00912d.
[6] M.D. Norling, F. Clayer, C.B. Gundersen, Levels of nitramines and nitrosamines in lake drinking water close to a CO_2 capture plant: a modelling perspective, Environ. Res. 212 (2022), 113581, https://doi.org/10.1016/j.envres.2022.113581.
[7] C.-C. Fan, T.-F. Lin, N-nitrosamines in drinking water and beer: detection and risk assessment, Chemosphere 200 (2018) 48–56, https://doi.org/10.1016/j.chemosphere.2018.02.025.
[8] M. Lashgari, Y. Yamini, C. Basheer, H.K. Lee, Ordered mesoporous carbon as sorbent for the extraction of N-nitrosamines in wastewater and swimming pool water, J. Chromatogr. A 1513 (2017) 35–41, https://doi.org/10.1016/j.chroma.2017.07.046.
[9] Z. Li, J. Wang, X. Chen, S. Hu, T. Gong, Q. Xian, A novel molecularly imprinted polymer-solid phase extraction method coupled with high performance liquid chromatography tandem mass spectrometry for the determination of nitrosamines in water and beverage samples, Food Chem. 292 (2019) 267–274, https://doi.org/10.1016/j.foodchem.2019.04.036.
[10] B. Li, M. Chen, Y. Li, X. Cao, Y. She, J. Yin, S. Cong, Z. Zhang, Preparation of flower-like molybdenum disulfide for solid-phase extraction of N-nitrosoamines in environmental water samples, J. Sep. Sci. 45 (2022) 752–759, https://doi.org/10.1002/jssc.202100788.
[11] Y. Zhang, Y.G. Zhao, N. Muhammad, M.L. Ye, Y. Zhu, Ultrasound-assisted synthesis of clover-shaped nano-titania functionalized covalent organic frameworks for the dispersive solid phase extraction of N-nitrosamines in drinking water, J. Chromatogr. A 1618 (2020), 460891, https://doi.org/10.1016/j.chroma.2020.460891.
[12] M.M. Sanagi, M.H. Chong, S. Endud, W.A. Wan Ibrahim, I. Ali, Nano iron porphyrinated poly(amidoamine) dendrimer mobil composition matter-41 for extraction of N-nitrosodiphenylamine nitrosamine from water samples, Microporous Mesoporous Mater. 213 (2015) 68–77, https://doi.org/10.1016/j.micromeso.2015.04.011.
[13] Z. Talebpour, S. Rostami, H. Rezadoost, Evaluation of a method for the simultaneous quantification of N-nitrosamines in water samples based on stir bar sorptive extraction combined with high-performance liquid chromatography and diode array detection, J. Sep. Sci. 38 (2015) 1601–1609, https://doi.org/10.1002/jssc.201401290.
[14] F. Riazi Kermani, J. Pawliszyn, Sorbent coated glass wool fabric as a thin film microextraction device, Anal. Chem. 84 (2012) 8990–8995, https://doi.org/10.1021/ac301861z.
[15] A. Yahaya, D. Babatunde, L.W.B. Olaniyan, O. Agboola, Application of chromatographic techniques in the analysis of total nitrosamines in water, Heliyon 6 (2020), e03447, https://doi.org/10.1016/j.heliyon.2020.e03447.
[16] S. Hashemi, J.H. Park, M. Yang, J. Kim, Y. Oh, H. Pyo, J. Yang, Long-term monitoring and risk assessment of N-nitrosamines in the finished water of drinking water treatment plants in South Korea, Environ. Sci. Pollut. Res. 29 (2022) 3930–3943, https://doi.org/10.1007/s11356-021-15814-1.
[17] J.W. Munch, M.V. Bassett, Method 521:Determination of Nitrosamines in Drinking Water by Solid Phase Extraction and Capillary Column Gas Chromatography with Large Volume Injection and Chemical Ionization Tandem Mass Spectrometry (MS/MS), U.S. Environmental Protection Agency, 2004, pp. 1–47.
[18] H. Xu, K.S. Suslick, Water-soluble fluorescent silver nanoclusters, Adv. Mater. 22 (2010) 1078–1082, https://doi.org/10.1002/adma.200904199.
[19] N. Cao, J. Xu, H. Zhou, Y. Zhao, J. Xu, J. Li, S. Zhang, A fluorescent sensor array based on silver nanoclusters for identifying heavy metal ions, Microchem. J. 159 (2020), 105406, https://doi.org/10.1016/j.microc.2020.105406.
[20] W. Li, X. Zhang, X. Hu, Y. Shi, W. Xin, N. Liang, T. Shen, J. Xiao, M. Daglia, X. Zou, J. Shi, Dual modes of fluorescence sensing and smartphone readout for sensitive and visual detection of mercury ions in Porphyra, Anal. Chim. Acta 1226 (2022), 340153, https://doi.org/10.1016/j.aca.2022.340153.
[21] Y. Xu, J. Yan, Y. Zhu, H. Chen, C. Wu, X. Zhu, Y. Zhang, H. Li, M. Liu, S. Yao, Self-cascade nanoenzyme of cupric oxide nanoparticles (CuO NPs) induced in situ catalysis formation of polyelectrolyte as template for the synthesis of near-infrared fluorescent silver nanoclusters and the application in glutathione detection and bioimagi, Anal. Chem. 94 (2022), https://doi.org/10.1021/acs.analchem.2c02832, 14642–12651.
[22] K. Chaiendoo, S. Sooksin, S. Kulchat, V. Promarak, T. Tuntulani, W. Ngeontae, A new formaldehyde sensor from silver nanoclusters modified Tollens' reagent, Food Chem. 255 (2018) 41–48, https://doi.org/10.1016/j.foodchem.2018.02.030.
[23] P. Zhang, C. Jia, Y. Zhao, H. Luo, X. Tan, X. Ma, Y. Wang, Detection of tiopronin in body fluids and pharmaceutical products using red-emissive DNA-stabilized silver nanoclusters as a fluorescent probe, Microchim. Acta 186 (2019) 609, https://doi.org/10.1007/s00604-019-3730-0.
[24] L. Liu, Q. Zhang, F. Li, M. Wang, J. Sun, S. Zhu, Fluorescent DNA-templated silver nanoclusters for highly sensitive detection of D-penicillamine, Spectrochim. Acta, Part A 253 (2021), 119584, https://doi.org/10.1016/j.saa.2021.119584.
[25] Y. Zhao, H. Liu, Y. Jiang, S. Song, Y. Zhao, C. Zhang, J. Xin, B. Yang, Q. Lin, Detection of various biomarkers and enzymes via a nanocluster-based fluorescence turn-on sensing platform, Anal. Chem. 90 (2018) 14578–14585, https://doi.org/10.1021/acs.analchem.8b04691.
[26] Y. Hu, J. Liu, J. Li, T. Chen, M. Wu, Dual-functional imprinted magnetic nanoprobes for fluorescence detection of: N -nitrosodiphenylamine, Anal. Methods 10 (2018) 2384–2389, https://doi.org/10.1039/c8ay00584b.
[27] C. Lee, W. Choi, Y.G. Kim, J. Yoon, UV photolytic mechanism of N-nitrosodimethylamine in water: dual pathways to methylamine versus dimethylamine, Environ. Sci. Technol. 39 (2005) 2101–2106, https://doi.org/10.1021/es0488941.
[28] S. Goldstein, D. Behar, T. Rajh, J. Rabani, Nitrite reduction to nitrous oxide and ammonia by TiO_2 electrons in a colloid solution via consecutive one-electron transfer reactions, J. Phys. Chem. A 120 (2016) 2307–2312, https://doi.org/10.1021/acs.jpca.6b01761.
[29] M. Lee, Y. Lee, F. Soltermann, U. von Gunten, Analysis of N-nitrosamines and other nitro(so) compounds in water by high-performance liquid chromatography with post-column UV photolysis/Griess reaction, Water Res. 47 (2013) 4893–4903, https://doi.org/10.1016/j.watres.2013.05.031.
[30] J.E. Grebel, I.H. Suffet, Nitrogen-phosphorus detection and nitrogen chemiluminescence detection of volatile nitrosamines in water matrices: optimization and performance comparison, J. Chromatogr. A 1175 (2007) 141–144, https://doi.org/10.1016/j.chroma.2007.09.073.
[31] F. Breider, U. Von Gunten, Quantification of total N-nitrosamine concentrations in aqueous samples via UV-photolysis and chemiluminescence detection of nitric oxide, Anal. Chem. 89 (2017) 1574–1582, https://doi.org/10.1021/acs.analchem.6b03595.
[32] S.L. Roback, H. Kodamatani, T. Fujioka, M.H. Plumlee, Validation of a novel direct-injection chemiluminescence-based method for: N-nitrosamine analysis in advanced-treated recycled water, drinking water, and wastewater, Environ. Sci. Water Res. Technol. 6 (2020) 1106–1115, https://doi.org/10.1039/c9ew00943d.
[33] F. Lu, S. Zhou, J.J. Zhu, Photochemical synthesis of fluorescent Ag nanoclusters and enhanced fluorescence by ionic liquid, Int. J. Hydrogen Energy 38 (2013) 13055–13061, https://doi.org/10.1016/j.ijhydene.2013.03.081.
[34] V. Romero, I. Costas-Mora, I. Lavilla, C. Bendicho, Facile preparation of an immobilized surfactant-free palladium nanocatalyst for metal hydride trapping: a novel sensing platform for TXRF analysis, Nanoscale 7 (2015) 1994–2002, https://doi.org/10.1039/c4nr05755d.
[35] F. Zhang, Y. Pi, J. Cui, Y. Yang, X. Zhang, N. Guan, Unexpected selective photocatalytic reduction of nitrite to nitrogen on silver-doped titanium dioxide, J. Phys. Chem. C 111 (2007) 3756–3761, https://doi.org/10.1021/jp067807j.
[36] S. Rengaraj, X.Z. Li, Enhanced photocatalytic reduction reaction over Bi^{3+}-TiO_2 nanoparticles in presence of formic acid as a hole scavenger, Chemosphere 66 (2007) 930–938, https://doi.org/10.1016/j.chemosphere.2006.06.007.
[37] C. Bendicho, F. Pena, M. Costas, S. Gil, I. Lavilla, Photochemistry-based sample treatments as greener approaches for trace-element analysis and speciation, TrAC, Trends Anal. Chem. 29 (2010) 681–691, https://doi.org/10.1016/j.trac.2010.05.003.
[38] B. Barrios, D. Kamath, E. Coscarelli, D. Minakata, Elementary reaction-based kinetic model for the fate of: N-nitrosodimethylamine under UV oxidation, Environ. Sci. Water Res. Technol. 7 (2021) 1748–1759, https://doi.org/10.1039/d1ew00262g.
[39] N. Tong, Z. Xia, T. Xie, X. Liu, J. Shen, Z. Zhang, X. Wang, Photochemistry of nitrate ion: reduction by formic acid under UV irradiation, Photochem. Photobiol. 98 (2022) 404–411, https://doi.org/10.1111/php.13518.

[40] Y.A. Olcer, M. Tascon, A.E. Eroglu, E. Boyacı, Thin film microextraction: towards faster and more sensitive microextraction, TrAC, Trends Anal. Chem. 113 (2019) 93–101, https://doi.org/10.1016/j.trac.2019.01.022.
[41] Y. Yong, X. Lou, S. Li, C. Yang, X. Yin, Direct simulation of the influence of the pore structure on the diffusion process in porous media, Comput. Math. Appl. 67 (2014) 412–423, https://doi.org/10.1016/j.camwa.2013.08.032.
[42] E. Bahadori, M. Compagnoni, A. Tripodi, F. Freyria, M. Armandi, B. Bonelli, G. Ramis, I. Rossetti, Photoreduction of nitrates from waste and drinking water, Mater. Today Proc. 5 (2018) 17404–17413, https://doi.org/10.1016/j.matpr.2018.06.042.
[43] H.O.N. Tugaoen, S. Garcia-Segura, K. Hristovski, P. Westerhoff, Challenges in photocatalytic reduction of nitrate as a water treatment technology, Sci. Total Environ. 599–600 (2017) 1524–1551, https://doi.org/10.1016/j.scitotenv.2017.04.238.
[44] H. Shin, S. Jung, S. Bae, W. Lee, H. Kim, Nitrite reduction mechanism on a Pd surface, Environ. Sci. Technol. 48 (2014) 12768–12774, https://doi.org/10.1021/es503772x.
[45] Y. Ding, W. Sun, W. Yang, Q. Li, Formic acid as the in-situ hydrogen source for catalytic reduction of nitrate in water by PdAg alloy nanoparticles supported on amine-functionalized SiO_2, Appl. Catal. B Environ. 203 (2017) 372–380, https://doi.org/10.1016/j.apcatb.2016.10.048.
[46] E. Choi, K. Park, H. Lee, M. Cho, S. Ahn, Formic acid as an alternative reducing agent for the catalytic nitrate reduction in aqueous media, J. Environ. Sci. 25 (2013) 1696–1702, https://doi.org/10.1016/S1001-0742(12)60226-5.
[47] T. Górecki, J. Pawliszyn, Effect of sample volume on quantitative analysis by solid-phase microextraction: Part 1. Theoretical considerations, Analyst 122 (1997) 1079–1086, https://doi.org/10.1039/a701303e.
[48] A.L. Theis, A.J. Waldack, S.M. Hansen, M.A. Jeannot, Headspace solvent microextraction, Anal. Chem. 73 (2001) 5651–5654, https://doi.org/10.1021/ac015569c.
[49] A. Aqeel, C.-J. Kim, H.-J. Lim, Influence of pH on the UV photolysis of N-nitrosamines in water: kinetics and products, Int. J. Greenhouse Gas Control 64 (2017) 194–203, https://doi.org/10.1016/j.ijggc.2017.07.002.
[50] A. Ludviksson, C. Huang, H.J. Jänsch, R.M. Martin, Isotopic studies of the reaction of NO on silver surfaces, Surf. Sci. 284 (1993) 328–336, https://doi.org/10.1016/0039-6028(93)90503-C.
[51] G. Rodríguez-Gattorno, D. Díaz, L. Rendón, G.O. Hernández-Segura, Metallic nanoparticles from spontaneous reduction of silver(I) in DMSO. Interaction between nitric oxide and silver nanoparticles, J. Phys. Chem. B 106 (2002) 2482–2487, https://doi.org/10.1021/jp012670c.
[52] J. Zhang, Q. Gao, X.M. Li, J.Z. Zhou, X.X. Ruan, Q. Liu, G.R. Qian, Z.P. Xu, Role of carboxylic acid groups in the reduction of nitric oxide by carbon at low temperature, as exemplified by graphene oxide, Phys. Chem. Chem. Phys. 19 (2017) 22462–22471, https://doi.org/10.1039/c7cp01541k.
[53] M. Han, M. Jafarikojour, M. Mohseni, The impact of chloride and chlorine radical on nitrite formation during vacuum UV photolysis of water, Sci. Total Environ. 760 (2021), 143325, https://doi.org/10.1016/j.scitotenv.2020.143325.
[54] New Hampshire Department of Environmental Science, Environmental Fact Sheet - Sodium and Chloride in Drinking Water, 2010. http://des.nh.gov/organization/commissioner/pip/factsheets/dwgb/documents/dwgb-3-17.pdf.
[55] United States Environmental Protection Agency, Drinking Water Advisory: Consumer Acceptability Advice and Health Effects Analysis on Methyl Tertiary-Butyl Ether (MTBE), 2003. EPA-822-R-03-006.
[56] Y. Qian, M. Wu, W. Wang, B. Chen, H. Zheng, S.W. Krasner, S.E. Hrudey, X.-F. Li, Determination of 14 nitrosamines at nanogram per liter levels in drinking water, Anal. Chem. 87 (2015) 1330–1336, https://doi.org/10.1021/ac504104k.
[57] Y. Kadmi, L. Favier, I. Soutrel, M. Lemasle, D. Woldbert, Ultratrace-level determination of N-Nitrosodimethylamine, N-Nitrosodiethylamine, and N-Nitrosomorpholine in waters by solid-phase extraction followed by liquid chromatography-tandem mass spectrometry, Cent. Eur. J. Chem. 12 (2014) 928–936, https://doi.org/10.2478/s11532-014-0537-z.
[58] H. Kodamatani, H. Yamasaki, T. Sakaguchi, S. Itoh, Y. Iwaya, M. Saga, K. Saito, R. Kanzaki, T. Tomiyasu, Rapid method for monitoring N-nitrosodimethylamine in drinking water at the ng/L level without pre-concentration using high-performance liquid chromatography-chemiluminescence detection, J. Chromatogr. A 1460 (2016) 202–206, https://doi.org/10.1016/j.chroma.2016.07.014.
[59] K. Alhooshani, Determination of N-nitrosamines in water resources using Al-AC sorbent for stir-bar supported micro-solid-phase extraction coupled with gas chromatography mass-spectrometry, Microchem. J. 146 (2019) 622–629, https://doi.org/10.1016/j.microc.2019.01.061.